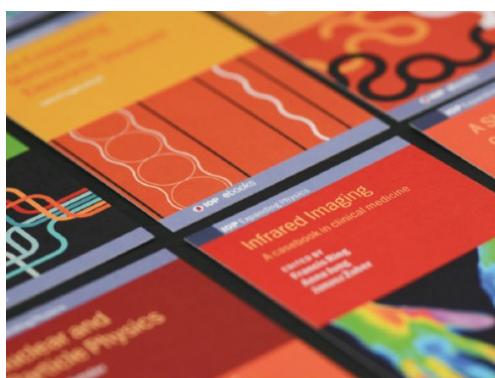


PAPER

## Diamond thin films integrated with flexible substrates and their physical, chemical and biological characteristics

To cite this article: Yang Xie *et al* 2021 *J. Phys. D: Appl. Phys.* **54** 384004

View the [article online](#) for updates and enhancements.





**IOP | ebooks™**

Bringing together innovative digital publishing with leading authors from the global scientific community.

Start exploring the collection—download the first chapter of every title for free.

# Diamond thin films integrated with flexible substrates and their physical, chemical and biological characteristics

Yang Xie<sup>1</sup>, Huachun Wang<sup>1</sup>, Dali Cheng<sup>1</sup>, He Ding<sup>2</sup>, Deying Kong<sup>3</sup>, Lizhu Li<sup>1</sup>, Lan Yin<sup>3</sup>, Guanlei Zhao<sup>4</sup>, Lei Liu<sup>4</sup>, Guisheng Zou<sup>4</sup>, Junjun Wei<sup>5</sup>, Chengming Li<sup>5</sup> , Changbo Liu<sup>6,\*</sup> and Xing Sheng<sup>1,\*</sup> 

<sup>1</sup> Department of Electronic Engineering, Beijing National Research Center for Information Science and Technology, Center for Flexible Electronics Technology, Tsinghua University, Beijing 100084, People's Republic of China

<sup>2</sup> Beijing Engineering Research Center of Mixed Reality and Advanced Display, School of Optics and Photonics, Beijing Institute of Technology, Beijing 100081, People's Republic of China

<sup>3</sup> School of Materials Science and Engineering, Tsinghua University, Beijing 100084, People's Republic of China

<sup>4</sup> Department of Mechanical Engineering, Tsinghua University, Beijing 100084, People's Republic of China

<sup>5</sup> Institute for Advanced Materials and Technology, University of Science and Technology Beijing, Beijing 100083, People's Republic of China

<sup>6</sup> School of Materials Science and Engineering and Hangzhou Innovation Institute, Beihang University, Beijing 100191, People's Republic of China

E-mail: [liuchb@buaa.edu.cn](mailto:liuchb@buaa.edu.cn) and [xingsheng@tsinghua.edu.cn](mailto:xingsheng@tsinghua.edu.cn)

Received 31 March 2021, revised 31 May 2021

Accepted for publication 23 June 2021

Published 9 July 2021



CrossMark

## Abstract

Diamond has attracted tremendous attention in materials science and engineering, owing to its superior mechanical, thermal, electrical and optical properties. However, its applications in biomedical fields are constrained by its mechanical rigidity, high temperature fabrication and difficulties of integration with flexible platforms. In this paper, we develop a facile process to form large-area, freestanding diamond thin films and combine them with optoelectronic devices on flexible substrates. Obtained undoped diamond (UD) and boron doped diamond (BDD) films are comprehensively investigated, in terms of their structural, morphological, optical and electrochemical characteristics. On flexible substrates, electrically conductive BDD films are employed as an electrochemical sensor for dopamine detection in aqueous solutions, while optically transparent and thermally conductive UD films can effectively promote heat dissipation of microscale light-emitting diodes. Finally, *in vitro* cytotoxicity study demonstrates the desirable biocompatibility of these diamond films. The presented techniques remove barriers in the manufacturing and heterogeneous integration of freestanding thin-film diamond materials, and provide promising paths to their broad applications in flexible biointegrated systems.

Keywords: diamond, flexible electronics, transfer printing

(Some figures may appear in color only in the online journal)

\* Authors to whom any correspondence should be addressed.

## 1. Introduction

Over the past decades, diamond has been regarded as an important engineering material [1] and received tremendous attention due to its ultrahigh thermal conductivity [2, 3], ultrawide bandgap [4], superior hardness [5], broadband optical transparency [6] and desirable chemical stability [7]. It has been widely explored for academic research and industrial development, from conventional applications like mechanical processing [8, 9] and heat management packaging [10, 11], to emerging studies include high-power electronics [12–15] and quantum computing [16, 17].

More recently, diamond-based materials have also found particular interests in biological fields. For example, because of its broadband optical transparency and ultrahigh thermal conductivity, undoped diamond (UD) can be integrated with optogenetic devices like light-emitting diodes (LEDs) to facilitate heat dissipation during operation [18]. In addition, boron doped diamond (BDD) exhibits superior electrochemical properties including wide electrochemical window, low impedance, and high corrosion resistance, leading to an ideal solution to biological and chemical sensors [19, 20]. Furthermore, the desirable biocompatibility and aqueous stability of diamond endow it with great potential for biomedical and specifically implantable devices [21–23]. Recently reported examples include electrochemical detectors [20, 24], BDD-based implantable biochemical sensors [25, 26], and our recently developed wireless, implantable optoelectrochemical probe for optogenetic stimulation and dopamine (DA) detection with combined LEDs and diamond [27].

Despite its unique features, the utilization of diamond for widespread biomedical applications is still limited by its processing technologies and difficulties in its integration with heterogeneous devices and substrates. High-quality diamond thin films are commonly synthesized on rigid substrates like silicon or molybdenum via chemical vapor deposition (CVD) at elevated temperatures (500 °C–1200 °C) with potential uses of plasma bombardment [28], which impedes their integration with flexible, bendable, and biocompatible for wearable or implantable uses [29]. Practical methods for preparing freestanding diamond thin films were previously demonstrated by growing and patterning CVD diamond on silicon dioxide (SiO<sub>2</sub>) coated Si substrates, and subsequently separating the film from origin substrates by removing the SiO<sub>2</sub> sacrificial layer in hydrofluoric acid (HF) [20, 25, 30, 31]. These demonstrated technologies typically require relatively complex multi-step fabrication and patterning, which is also difficult to achieve films with large areas. Prior arts also demonstrate thin-film diamond materials peeled off from quartz [32, 33] and tantalum [34–36], by employing low adhesion interfaces between diamond films and substrates during growth. The size of diamond membranes could be constrained by the substrates. Therefore, it is desirable to realize large-scale, freestanding diamond thin films, which can be further combined with heterogeneous devices and substrates for potential biointegration.

In this paper, we develop materials and process strategies to form both UD and BDD thin films via a simplified and efficient

approach, and heterogeneously integrate them with flexible substrates and optoelectronic devices. Surface morphologies, structural and optical properties of these films are experimentally investigated. Furthermore, we demonstrate their capabilities of electrochemical sensing of DA with BDD films and heat dissipation of microscale LEDs (micro-LEDs) with UD films. Finally, cell culture studies *in vitro* illustrate the biocompatibility of released diamond films. These results offer simple and reliable routes to various types of diamond membranes that are manufacturable, transferable, and biocompatible, and provide unprecedented opportunities for high performance biointegrated systems.

## 2. Experiments and results

Figure 1(a) schematically illustrates the process flow to form the large-area, freestanding diamond films. The fabrication begins with growing diamond thin films (with a thickness of  $\sim 10 \mu\text{m}$ ) on single crystalline silicon (100) substrates (with a diameter of 50 mm) via CVD. Before growth, Si substrates are abraded by sand paper (800#) and then cleaned ultrasonically in acetone for 15 min. The diamond films are synthesized by using a microwave plasma CVD system with a plasma frequency of 2.45 GHz. CH<sub>4</sub> and H<sub>2</sub> are fed into the chamber with a total reactor pressure of 40 Torr. Deposition temperature is 800 °C, and deposition rate is  $\sim 2 \mu\text{m h}^{-1}$ . For the BDD film deposition, the B<sub>2</sub>H<sub>6</sub> diluted by H<sub>2</sub> to 2 vol% is used as the doping source. The boron to carbon atom ratio in the react gas is 5000 ppm. After cleaning the as-grown diamond with acetone, isopropyl alcohol and deionized (DI) water, an adhesive stamp made of polydimethylsiloxane (PDMS) elastomer is attached to the top side of the diamond membrane, serving as a temporary holder during the etching process of the sacrificial substrate. Followed by immersing the Si wafers in an etchant solution (CH<sub>3</sub>COOH:HNO<sub>3</sub>:HF = 5:5:5, by volume) for half an hour to completely remove the Si substrate, large-area and freestanding diamond films are obtained and attached on PDMS. Via transfer printing, diamond thin films released from original Si substrates can be heterogeneously integrated onto any foreign substrates of interest. Representative images of released diamond films (thickness  $\approx 10 \mu\text{m}$ ; size  $\approx 1 \text{cm}^2$ ) on flexible PDMS and polyethylene terephthalate (PET) substrates are shown in figures 1(b) and (c), respectively. It is noted that these 10  $\mu\text{m}$  thick diamond membranes bonded on flexible sheets certainly do not possess ideal mechanical performance under bending and could be easily fractured. The flexibility of these heterogeneous structures with rigid diamond films can be further optimized, with examples that can be found in other inorganic materials like silicon and glass, by reducing the diamond film size and thickness [37], placing the diamond layer in the neutral plane [38] or adapting serpentine structures [39], etc. Laser milling can be applied to form diamond films with designed sizes and shapes for various purposes, as depicted in figure 1(d). Here the diamond films are patterned on silicon growth wafers prior to the wet etching, with a Nd:YVO<sub>4</sub> laser (wavelength 1064 nm, peak power 7 W, pulse repetition rate 1 MHz, scan speed 1 m s<sup>-1</sup>, and

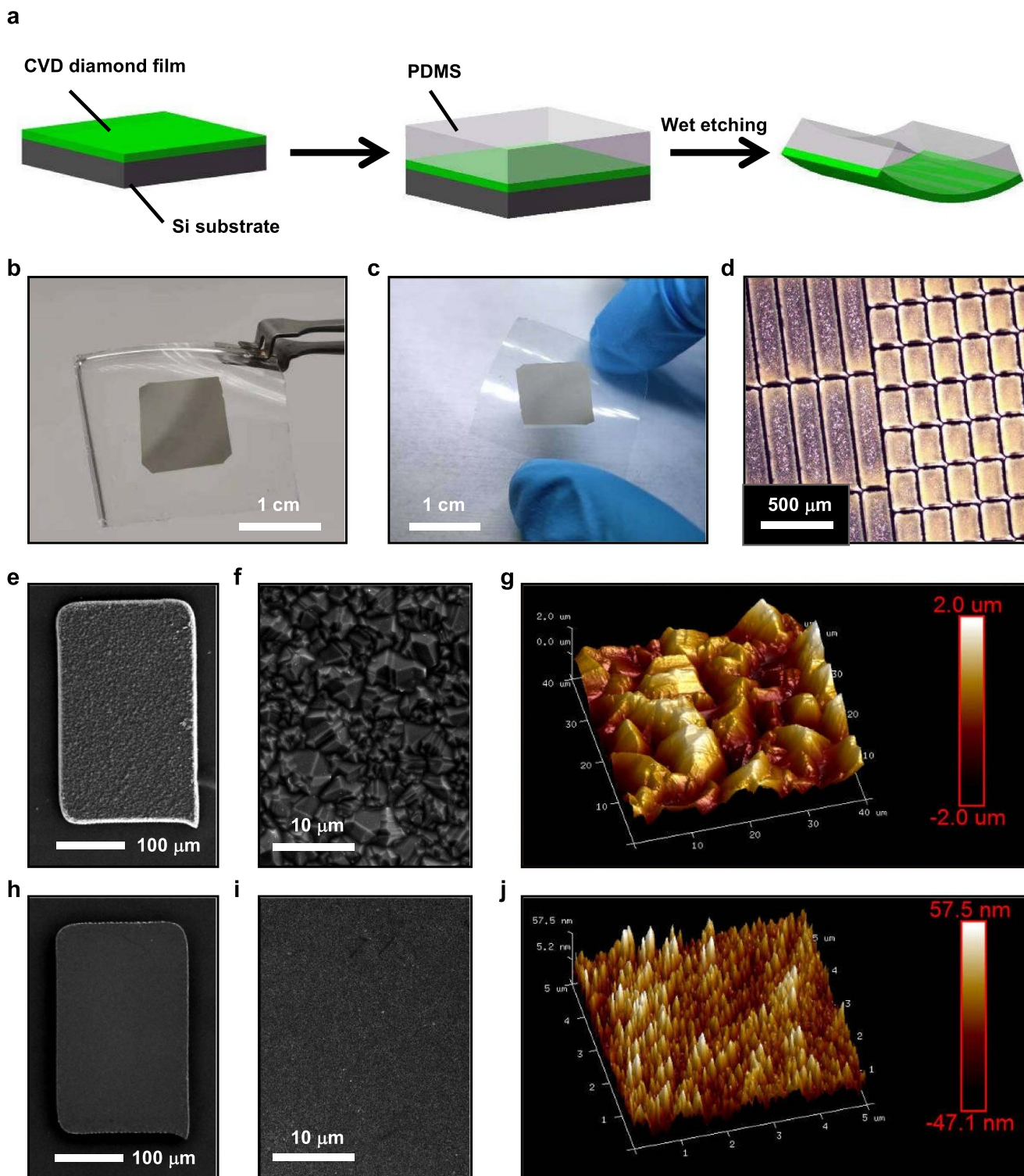


**Figure 1.** (a) Schematic illustration of processing flow for diamond film fabrication, including CVD, Si substrate etching and transfer printing. (b) and (c) Freestanding diamond films on (b) PDMS and (c) PET based flexible substrates. (d) Micrograph of thin-film diamond arrays formed by laser milling. (e)–(j) SEM and AFM images for (e)–(g) front and (h)–(j) back sides of a freestanding diamond film.

scan repetition 200 times). Surface morphologies of released diamond films are examined with scanning electron microscopy (SEM, Merlin VP Compact, Zeiss) and atomic force microscopy (AFM, Multimode 8 SPM, Bruker), as illustrated in figures 1(e)–(j). Due to the abnormal grain growth of the

polycrystalline films, the front and back sides of the diamond film exhibit significantly different surface morphologies [25, 40–43]. The front side of the sample that exposes to air has an obviously larger average grain size than the back side that interfaces with the Si substrate, thereby resulting in a larger

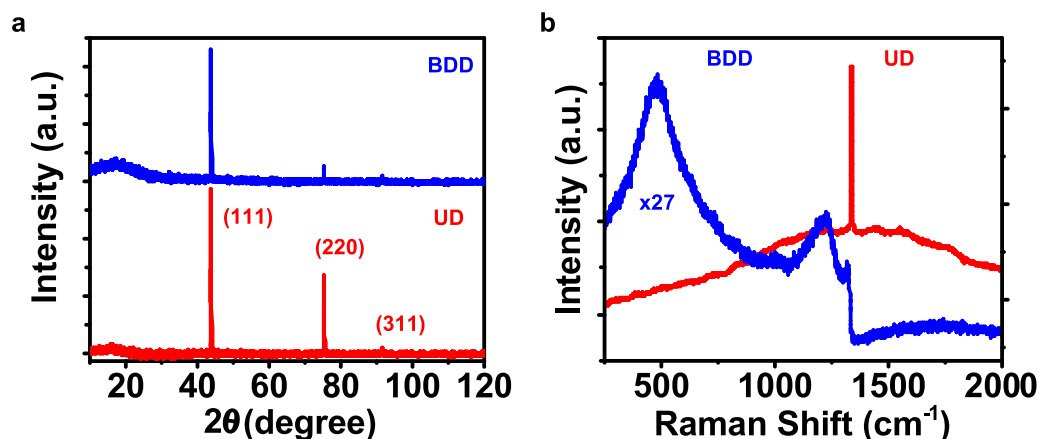


Figure 2. (a) XRD patterns and (b) Raman spectra of UD and BDD films.

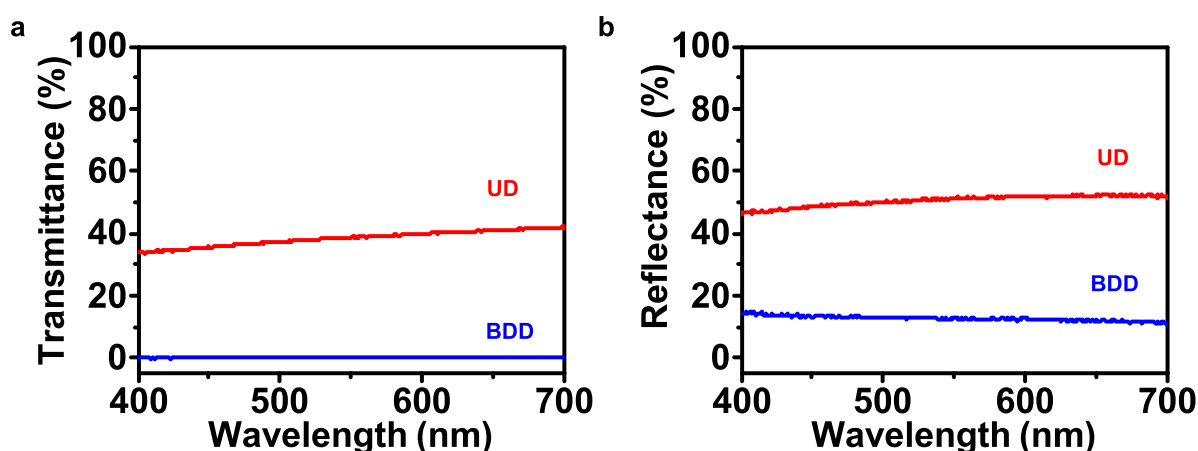


Figure 3. (a) Transmittance and (b) reflectance spectrum for UD and BDD film in the visible range.

roughness (root mean square roughness: 783 nm for front side versus 24 nm for back side).

Through the abovementioned film growth and release processes, both UD and BDD (doping concentration  $\sim 10^{21} \text{ cm}^{-3}$ ) films can be fabricated. Structural characteristics of UD and BDD films are studied by x-ray diffraction (XRD) (SmartLab, Rigaku, with a  $\text{Cu K}\alpha$  source) and Raman spectroscopy (confocal microscope, iHR550, Horiba, with an excitation wavelength of 532 nm). The results are presented and compared in figure 2. As XRD patterns shown figure 2(a), both UD and BDD films have a polycrystalline diamond structure, with diffraction peaks at  $\sim 43.9^\circ$ ,  $\sim 75.3^\circ$  and  $\sim 91.5^\circ$ , corresponding to (111), (220) and (311) planes of diamond, respectively [44, 45]. Impacts of boron doping can be revealed more clearly in the Raman spectra (figure 2(b)). The UD film shows a single diamond ( $\text{sp}^3$  carbon bond) peak at approximately  $1332 \text{ cm}^{-1}$ , indicating a high degree of crystallinity and purity [46–49]. By contrast, the BDD film shows lower crystal quality and owns additional peaks at around  $472 \text{ cm}^{-1}$  and  $1220 \text{ cm}^{-1}$ , resulting from boron dopants incorporated into the lattice [50, 51]. Additionally, the diamond characteristic peak (related to the  $\text{sp}^3$  carbon bond) for BDD is downshifted to  $\sim 1305 \text{ cm}^{-1}$ , and considerably attenuated and broadened

due to the boron doping [28, 52, 53]. Moreover, the broadband signal from  $1450 \text{ cm}^{-1}$  to  $1750 \text{ cm}^{-1}$  can be attributed to the presence of impurities and defects accompanied by the lattice mismatch between boron and carbon [25, 54–56].

To evaluate the potential of these diamond films for optoelectronic applications, optical transmittance and reflectance spectra for UD and BDD films (thickness  $\sim 10 \mu\text{m}$ ) are measured, with a spectrophotometer (Cary 5000, Agilent) (figure 3). Because of the strong optical scattering induced by the rough surface, an integrating sphere accessory is employed to capture the diffused light. Resulting from the heavy boron doping, the released BDD film is optically opaque, with nearly 0% transmittance and less than 20% reflectance in the visible range. As a comparison, the UD film exhibits  $\sim 40\%$  transmittance and  $\sim 50\%$  reflectance from 400 nm to 700 nm, leading to an absorption loss of around 10%. The high transparency of the UD film suggests that it could serve as an optical window for optoelectronic devices on flexible platforms.

Accompanied by the strong optical losses, the heavy boron doping also induces a high electrical conductivity, which implies that the BDD film could work as an effective electrochemical sensor. In figure 4, we evaluate its sensing capability by detecting DA in aqueous solutions. Measured by

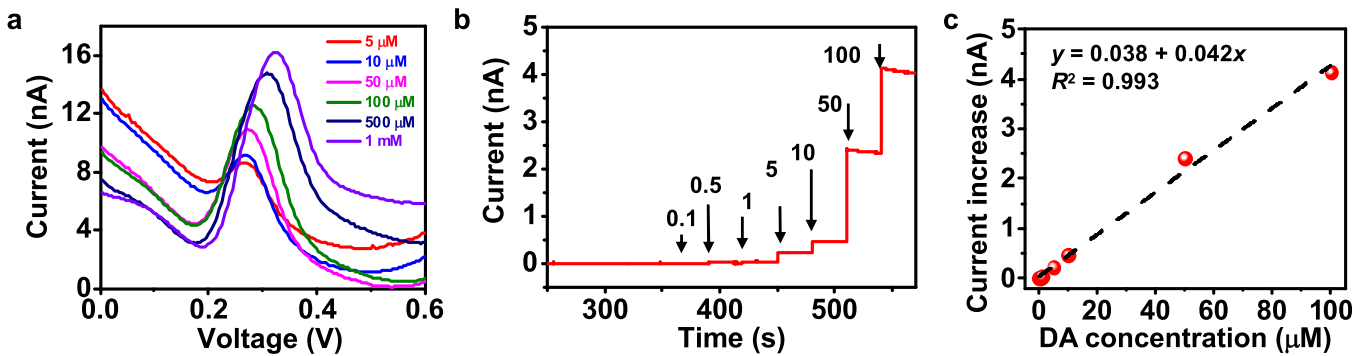


**Figure 4.** Electrochemical properties of a BDD film. (a) DPV curves of the film in aqueous solutions with various concentrations of DA. (b) CA curves of the BDD film in PBS solution with varied DA concentrations (unit:  $\mu\text{M}$ ). Insert: calibration curve, linear relationship between response currents and DA concentrations (0.1–100  $\mu\text{M}$ ).

a four-point probe tester (RTS-9, 4 PROBES TECH), the electrical resistivity of the BDD film transferred onto a flexible substrate is determined to be  $\sim 2.8 \times 10^{-5} \Omega \text{ m}$ . To form electrochemical sensors, BDD films with a size of  $150 \mu\text{m} \times 200 \mu\text{m}$  are transferred onto polyimide (PI) substrates, and metalized with sputter-coated Cr (5 nm)/Cu (600 nm)/Au (200 nm) films as contacts. Because of the large surface area, the front side of BDD diamond film is applied for chemical sensing. A photoresist film (SU-8, thickness 5  $\mu\text{m}$ ) serves as the protective coating on metal electrodes. The DA detection is performed with an electrochemical workstation (CHI 650E, Shanghai Chenhua Co., Ltd, China), with a standard three-electrode configuration. The BDD film, silver/silver chloride (Ag/AgCl) and platinum (Pt) serve as the working, the reference and the counter electrodes, respectively. A dilute hydrochloric acid (HCl) solution (pH = 4.0) is used as the solvent for DA, in order to mitigate its degradation due to natural oxidation in air [27, 57]. Differential pulse voltammetry (DPV) and chronoamperometry (CA) methods are utilized to analyze the electrochemical properties of the BDD film. In the DPV tests, measurement configurations are as follows: voltage step = 4 mV, pulse time = 200 ms, pulse amplitude = 50 mV, and HCl solutions have DA concentrations of 5  $\mu\text{M}$ , 10  $\mu\text{M}$ , 50  $\mu\text{M}$ , 100  $\mu\text{M}$ , 500  $\mu\text{M}$  and 1 mM. As shown in figure 4(a), well-defined oxidation peaks are observed in the presence of DA, with oxidation potentials of about 0.3 V, and peak oxidation currents increase with the DA concentration. The dynamic current response at varied DA concentrations is further analyzed using CA measurements at a fixed bias voltage of 0.6 V (figure 4(b)). As the DA concentration varies in the range of 0.1–100  $\mu\text{M}$ , recorded electrochemical current dynamically, resulting in a linear relation (figure 4(c)). The DA detection limit is determined to be around 5  $\mu\text{M}$ , and the detection sensitivity is  $\sim 0.045 \text{ nA } \mu\text{M}^{-1}$ . The normalized current response of DA by area is calculated to be  $\sim 150 \text{ nA } \mu\text{M cm}^{-2}$ , comparable with other studies [58]. The sensitivity of the BDD film is slightly lower than that of our previously reported UD diamond film coated with PEDOT:PSS [27]. By engineering the doping profile and surface modification (conducting polymers, metal nanoparticles, carbon-based materials, etc), these

diamond films can obtain further improved electrochemical performance, and find their use in biochemical detection *in vivo* [25, 59].

Patterned microscale UD films are heterogeneously integrated with micro-LEDs to exploit their optical and thermal features (figures 5 and 6). Schematically shown in figure 5(a), here we design and fabricate three different device configurations: a bare micro-LED on a copper (Cu; 18  $\mu\text{m}$ )/polyimide (PI; 25  $\mu\text{m}$ )/copper substrate (Cu; 18  $\mu\text{m}$ ), a micro-LED on diamond on Cu/PI/Cu, and a micro-LED with diamond on top on Cu/PI/Cu, and the smooth side of the UD film directly contacts with the micro-LED to minimize the diffuse reflection. For the blue micro-LEDs, their fabrication, transfer processes, electronic and optical characteristics can be found in previous reports [60, 61]. Corresponding photographs of the integrated needle-shape devices after laser milling are shown in figure 5(b). External quantum efficiencies (EQEs) for micro-LEDs in the above three different configurations are measured within an integrating sphere (Labsphere Inc.) and plotted as a function of injection currents in figure 5(c). The maximum EQE is  $\sim 12\%$  for the bare micro-LED and  $\sim 10\%$  for the micro-LED with diamond on top. The slight performance degradation (by  $\sim 20\%$ ) is in accordance with the low optical losses of the UD film (figure 3). For the micro-LED on diamond on Cu/PI/Cu, the maximum EQE is  $\sim 11\%$ , slightly lower than the bare LED due to the absorption of light transmitted from LED backside by defects in the diamond. Far-field angular emission profiles of the micro-LEDs with different configurations are measured and shown in figure 5(d). Here the devices are mounted onto a goniometer and the measurement is taken from  $-90^\circ$  to  $90^\circ$  in a step of  $5^\circ$ , at an injection current of 3 mA. The emission intensity is captured by a standard Si photodetector (DET36A, Thorlabs). The nearly Lambertian emission patterns are observed for all the devices. These results indicate that the diamond films integrated with the micro-LEDs do not greatly alter their emission characteristics.

Due to its ultrahigh thermal conductivity, diamond has been used as a heat spreader for high power devices, such as laser diodes and multichip modules [62]. Previously reported diamond films exhibit thermal conductivities ranging from

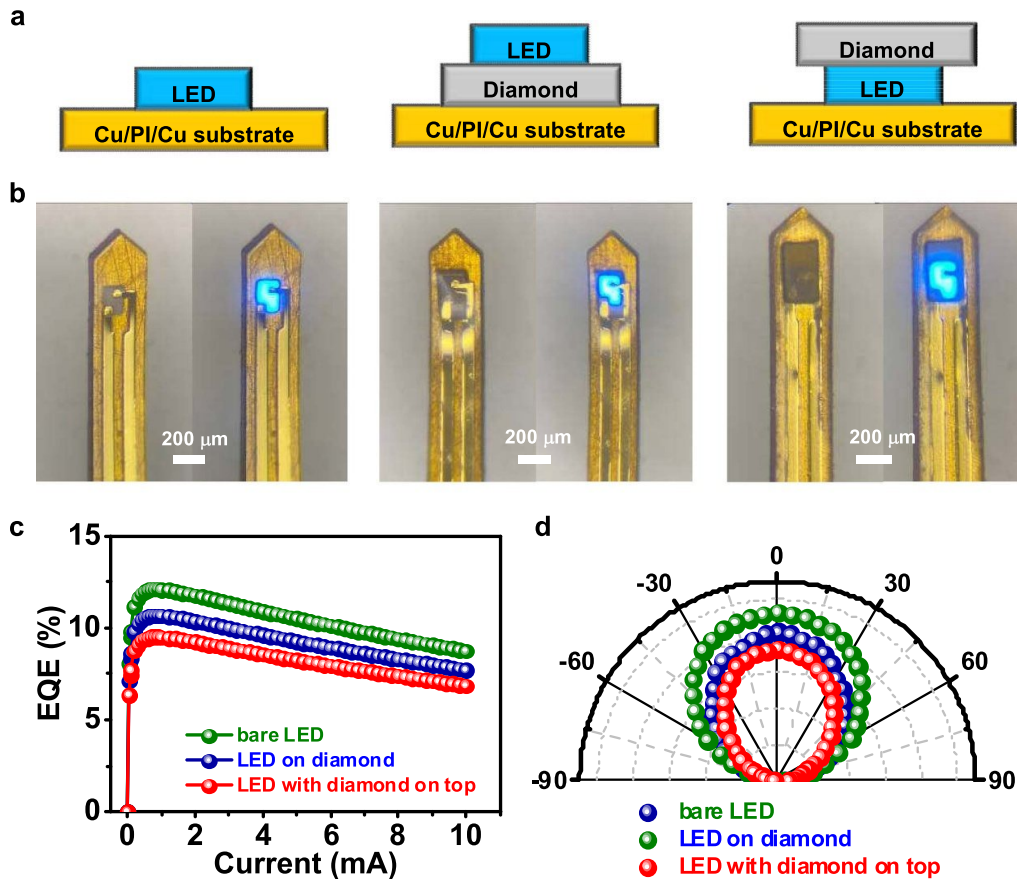


**Figure 5.** (a) Schematics and (b) corresponding images of UD films integrated with blue micro-LEDs. Left: a bare LED on the copper/polyimide/copper (Cu/PI/Cu) substrate; middle: an LED on diamond on Cu/PI/Cu; right: an LED with diamond on top on Cu/PI/Cu. (c) EQEs versus injection currents and (d) angular distribution of optical emissions for LEDs in different configurations.

$700 \text{ W m}^{-1} \text{ K}^{-1}$  to  $2200 \text{ W m}^{-1} \text{ K}^{-1}$  [3, 63–65], higher than metals like copper ( $395 \text{ W m}^{-1} \text{ K}^{-1}$ ) and orders of magnitude higher than that of organic coatings such as SU-8 and PDMS ( $<1 \text{ W m}^{-1} \text{ K}^{-1}$ ). Such a thermally conductive coating is advantageous for heat dissipation of micro-LEDs. In figure 6, we evaluate thermal behaviors of the micro-LEDs with different configurations using an infrared camera (FOTRIC 228) with a  $25 \mu\text{m}$  close-up lens, which is calibrated with a hot plate with standard digital temperature indicators. Meanwhile, numerical models based on finite element analysis (Comsol Multiphysics) are established to simulate the thermal distributions. In the thermal model, thermal conductivities for various materials are  $2000 \text{ W m}^{-1} \text{ K}^{-1}$  for diamond,  $0.15 \text{ W m}^{-1} \text{ K}^{-1}$  for PI and SU8,  $400 \text{ W m}^{-1} \text{ K}^{-1}$  for copper and  $0.16 \text{ W m}^{-1} \text{ K}^{-1}$  for PDMS. With micro-LEDs operated in ambient air under constant current injections varied from 0 to 10 mA, experimental and calculation results (figure 6(a)) suggest that the temperature rises during operation for micro-LEDs can be reduced by  $\sim 20\%$  at most, when integrating with UD films. We also note that the positions of the UD films have little effect on the maximum temperature rises for micro-LEDs. Measured and calculated thermal maps for micro-LED probes with different configurations are further depicted and compared in figures 6(b)–(d), under an injection current of 5 mA. These results show that the diamond obtained in this work

can effectively facilitate the heat dissipation of micro-LEDs, which is critically important for biomedical applications such as deep brain optogenetic stimulations, since the mitigation of unwanted abnormal activities and possible tissue damage by overheating is crucial for neural systems. Besides serving as an efficient heat sinker for devices on organic based substrates, other possibilities involve the development of diamond based high-power, high-speed electronic devices on flexible platforms [66, 67].

In order to reveal the biocompatibility of these diamond films, cytotoxicity tests are conducted by *in vitro* cell culturing and viability evaluations on the sample surfaces. Original UD and BDD films have hydrophobic surfaces [68, 69], which are undesirable for *in vitro* cell culturing. To promote cell adhesion and proliferation, all the diamond films are immersed in a DA solution ( $2 \text{ mg ml}^{-1}$  in  $10 \text{ mM}$  Tris-HCl buffer,  $\text{pH} = 8.5$ ) for 2 h to form a hydrophilic polydopamine coating [70] and rinsed three times with DI water to remove the unattached polydopamine molecules. Subsequently, UD and BDD films are sterilized in 75% ethanol for 15 min, followed by ultraviolet irradiation for 1 h. Human bone marrow-derived mesenchymal stem cells (hBMSCs) (#7500, ScienceCell, USA) are cultured in a mesenchymal stem cell medium (#7510, ScienceCell) with 10% fetal bovine serum and 1% penicillin–streptomycin in a humid atmosphere containing 5%

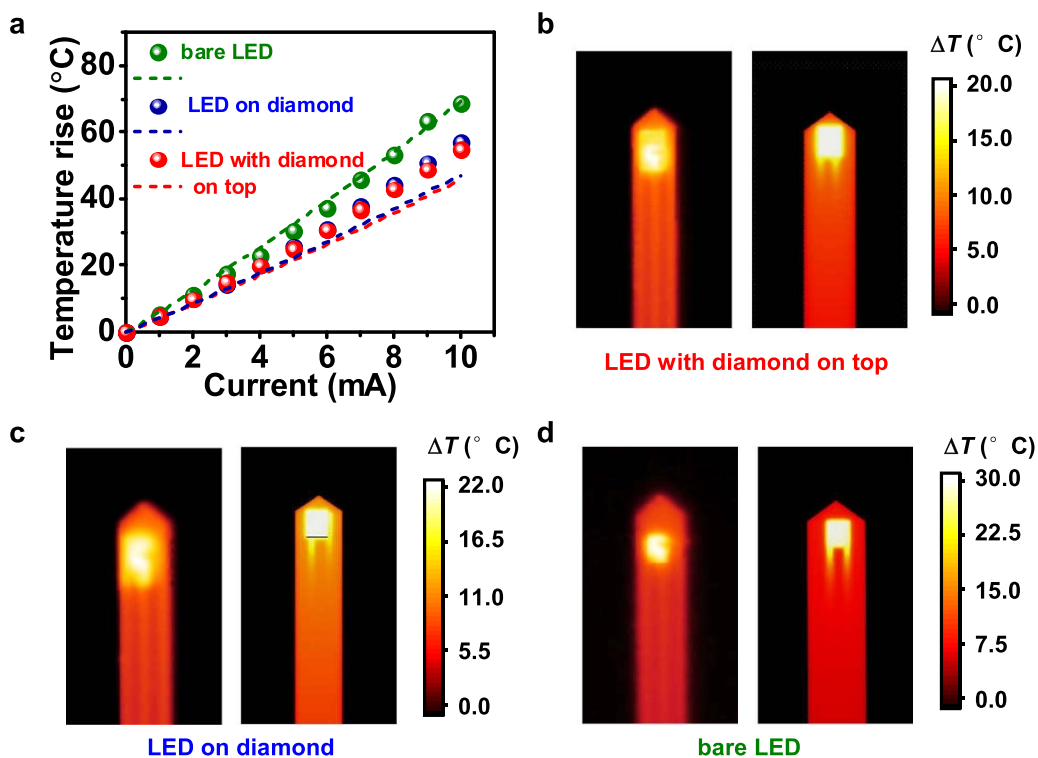


**Figure 6.** (a) Measured (dots) and simulated (dashed lines) maximum temperature rises above room temperature on the top surface of the LED probes integrating UD films with different configurations. (b)–(d) Measured (left) and simulated (right) temperature distributions for LED probes with different configurations (under an injection current of 5 mA): (b) LED with diamond on top, (c) LED on diamond and (d) bare LED.

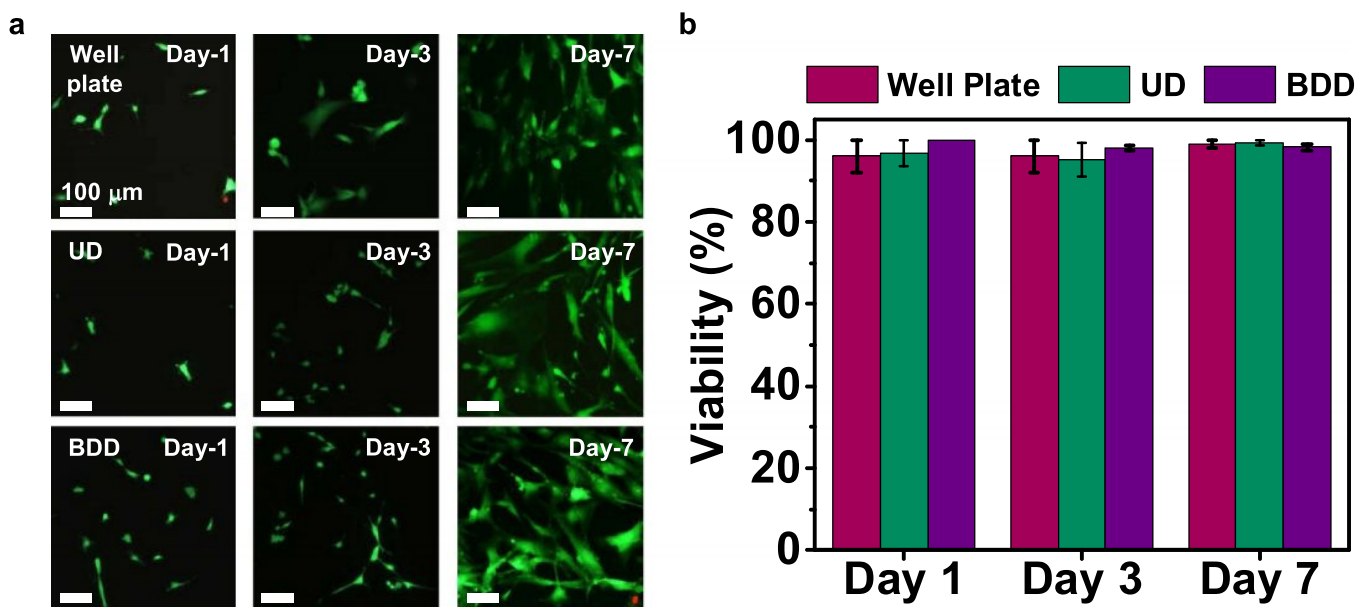


**Figure 7.** *In vitro* biocompatibility tests for UD and BDD films. (a) Fluorescent images showing the proliferation behaviors for hBMSCs at different time points. In a live/dead viability assay, living cells cause green fluorescence and dead cells cause red fluorescence. (b) Comparison of cell viability (percentage of living cells) after culturing for 1, 3, and 7 d. Results are presented as mean  $\pm$  standard deviation. ( $n = 3$  groups for each sample).



CO<sub>2</sub>. The cell culture medium is replaced every 2 d. Cultured hBMSCs are separately seeded on the rough side of UD, BDD and standard 48-well cell culture plate at a density of  $\sim 40$  cells mm<sup>-2</sup>. Live/dead staining is performed after the cells are cultured for 1, 3, and 7 d. Before the analysis of cell proliferation, all of the samples are washed with phosphate buffered saline (PBS) twice and stained with a calcein-AM (for live cells) and propidium iodide (for dead cells) mixed solution (KeyGEN BioTECH, China) for 30 min. A fluorescence microscope (Olympus) is used to observe the distribution of living and dead cells on the samples. Figure 7(a) shows the growth and proliferation behaviors of hBMSCs, as demonstrated by a set of representative fluorescent images on days 1, 4, and 7, and the living and dead cells are marked with green and red fluorescence, respectively. The statistical results (live/dead cell counting) are taken from fluorescence images in three different areas for each sample, and  $n = 3$  samples for both UD and BDD films. On the whole, the hBMSCs interact and adhere well to all of the samples, proliferating significantly within 7 d. In regards to the cellular morphologies and viabilities (between 89% and 100%), there are no significant difference among these three groups (figure 7(b)), which indicates an absence of cell toxic effects for diamond films throughout the duration of the experiment. *In vitro* cytotoxicity tests confirm that both UD and BDD films are fully biocompatible, which can be readily employed in implantable optoelectronic systems for biomedical uses, such as electrochemical sensing and optogenetic stimulation in neuroscience research.

### 3. Conclusion

In summary, we introduce a simplified fabrication approach to effectively form freestanding polycrystalline diamond thin films and deterministically implement them with flexible electronic systems. UD and BDD films are released from silicon substrates and comprehensively investigated in terms of their morphological, structural and optical properties, as well as their biocompatibilities. Large-area and freestanding diamond thin films are obtained and attached on flexible substrates. In flexible microsystems, microscale BDD sheets are integrated with flexible substrates for electrochemical demonstration, while thermal and optical properties of micro-LEDs probe integrated with UD films are systematically studied. With further size reduction, such diamond films can be integrated with microscale devices to realize flexible and multifunctional biomedical microsystems. By engineering the doping profile and surface modification, these diamond films can obtain further improved electrochemical performance, and find their use in biochemical detection *in vivo* [25, 59]. Besides serving as an efficient heat sinker for devices on organic based substrates, other possibilities involve the development of diamond based high-power, high-speed electronic devices on flexible platforms [66, 67]. Collectively, these material and device strategies provide promising paths to the broad applications of thin-film diamond in biointegrated systems.

### Data availability statement

All data that support the findings of this study are included within the article (and any supplementary files).

### Acknowledgments

The authors thank financial support from the National Natural Science Foundation of China (NSFC) (61874064 for X S, 62004009 for C L), Beijing Municipal Natural Science Foundation (4202032 for X S), the Beijing Innovation Center for Future Chips, Tsinghua University, and the Beijing National Research Center for Information Science and Technology (BNR2019ZS01005). We also thank Z Chen and H Zhang (Chinese Academy of Sciences) for the thermal conductance measurement.

### ORCID iDs

Chengming Li  <https://orcid.org/0000-0003-4401-6007>  
Xing Sheng  <https://orcid.org/0000-0002-8744-1700>

### References

- [1] May P W 2008 The new diamond age? *Science* **319** 1490
- [2] Wei L, Kuo P, Thomas R, Anthony T and Banholzer W 1993 Thermal conductivity of isotopically modified single crystal diamond *Phys. Rev. Lett.* **70** 3764
- [3] Hartmann J, Voigt P and Reichling M 1997 Measuring local thermal conductivity in polycrystalline diamond with a high resolution photothermal microscope *J. Appl. Phys.* **81** 2966–72
- [4] Watanabe H, Nebel C E and Shikata S 2009 Isotopic homojunction band engineering from diamond *Science* **324** 1425
- [5] Li Q, Zhan G, Li D, He D, Moellendick T E, Gooneratne C P and Alalsayednassir A G 2020 Ultrastrong catalyst-free polycrystalline diamond *Sci. Rep.* **10** 22020
- [6] Walker J 1979 Optical absorption and luminescence in diamond *Rep. Prog. Phys.* **42** 1605–59
- [7] Popov I V, Görne A L, Tchougréeff A L and Dronskowski R 2019 Relative stability of diamond and graphite as seen through bonds and hybridizations *Phys. Chem. Chem. Phys.* **21** 10961–9
- [8] Lee Y J, Hao L, Lüder J, Chaudhari A, Wang S, Manzhos S and Wang H 2019 Micromachining of ferrous metal with an ion implanted diamond cutting tool *Carbon* **152** 598–608
- [9] Kawasegi N, Ozaki K, Morita N, Nishimura K and Yamaguchi M 2017 Development and machining performance of a textured diamond cutting tool fabricated with a focused ion beam and heat treatment *Precis. Eng.* **47** 311–20
- [10] Eden R C 1993 Application of diamond substrates for advanced high density packaging *Diam. Relat. Mater.* **2** 1051–8
- [11] Zhang Y, Hu X, Zhao J H, Sheng K, Cannon W R, Wang X and Fursin L 2009 Rheology and thermal conductivity of diamond powder-filled liquid epoxy encapsulants for electronic packaging *IEEE Trans. Compon. Packag. Technol.* **32** 716–23
- [12] Chao P, Chu K, Creamer C, Diaz J, Yurovchak T, Shur M, Kallaher R, McGray C, Via G D and Blevins J D 2015 Low-temperature bonded GaN-on-diamond HEMTs with

- 11 W/mm output power at 10 GHz *IEEE Trans. Electron Devices* **62** 3658–64
- [13] Ohki T, Yamada A, Minoura Y, Makiyama K, Kotani J, Ozaki S, Sato M, Okamoto N, Joshin K and Nakamura N 2019 An over 20 W/mm S-band InAlGaN/GaN HEMT with SiC/diamond-bonded heat spreader *IEEE Electron Device Lett.* **40** 287–90
- [14] Goyal V, Sumant A V, Teweldebrhan D and Balandin A A 2012 Direct low-temperature integration of nanocrystalline diamond with GaN substrates for improved thermal management of high-power electronics *Adv. Funct. Mater.* **22** 1525–30
- [15] Shikata S 2016 Single crystal diamond wafers for high power electronics *Diam. Relat. Mater.* **65** 168–75
- [16] Liu K, Zhang S, Ralchenko V, Qiao P, Zhao J, Shu G, Yang L, Han J, Dai B and Zhu J 2021 Tailoring of typical color centers in diamond for photonics *Adv. Mater.* **33** 2000891
- [17] Lühmann T et al 2018 Screening and engineering of colour centres in diamond *J. Phys. D: Appl. Phys.* **51** 483002
- [18] Fan B, Kwon K-Y, Rechenberg R, Becker M F, Weber A J and Li W 2016 A hybrid neural interface optrode with a polycrystalline diamond heat spreader for optogenetics *Technology* **04** 15–22
- [19] Yang N, Foord J S and Jiang X 2016 Diamond electrochemistry at the nanoscale: a review *Carbon* **99** 90–110
- [20] Fan B, Zhu Y, Rechenberg R, Rusinek C A, Becker M F and Li W 2017 Large-scale, all polycrystalline diamond structures transferred onto flexible parylene-C films for neurotransmitter sensing *Lab Chip* **17** 3159–67
- [21] Alcaide M, Taylor A, Fjorback M, Zachar V and Pennisi C P 2016 Boron-doped nanocrystalline diamond electrodes for neural interfaces: *in vivo* biocompatibility evaluation *Front. Neurosci.* **10** 87
- [22] Yang K-H and Narayan R J 2019 Biocompatibility and functionalization of diamond for neural applications *Curr. Opin. Biomed. Eng.* **10** 60–8
- [23] Garrett D J, Tong W, Simpson D A and Meffin H 2016 Diamond for neural interfacing: a review *Carbon* **102** 437–54
- [24] Li H, Guo Y, Zeng S, Wei Q, Sharel P E, Zhu R, Cao J, Ma L, Zhou K and Meng L 2021 High-sensitivity, selective determination of dopamine using bimetallic nanoparticles modified boron-doped diamond electrode with anodic polarization treatment *J. Mater. Sci.* **56** 4700–15
- [25] Fan B et al 2020 Flexible, diamond-based microelectrodes fabricated using the diamond growth side for neural sensing *Microsyst. Nanoeng.* **6** 42
- [26] Ogata G et al 2017 A microsensing system for the *in vivo* real-time detection of local drug kinetics *Nat. Biomed. Eng.* **1** 654–66
- [27] Liu C et al 2020 A wireless, implantable optoelectrochemical probe for optogenetic stimulation and dopamine detection *Microsyst. Nanoeng.* **6** 64
- [28] Yang N, Yu S, Macpherson J V, Einaga Y, Zhao H, Zhao G, Swain G M and Jiang X 2019 Conductive diamond: synthesis, properties, and electrochemical applications *Chem. Soc. Rev.* **48** 157–204
- [29] Gracio J J, Fan Q H and Madaleno J C 2010 Diamond growth by chemical vapour deposition *J. Phys. D: Appl. Phys.* **43** 374017
- [30] Bergonzo P et al 2011 3D shaped mechanically flexible diamond microelectrode arrays for eye implant applications: the MEDINAS project *IRBM* **32** 91–4
- [31] Hess A E, Sabens D M, Martin H B and Zorman C A 2011 Diamond-on-polymer microelectrode arrays fabricated using a chemical release transfer process *J. Microelectromech. Syst.* **20** 867–75
- [32] Seshan V et al 2015 Pick-up and drop transfer of diamond nanosheets *Nanotechnology* **26** 125706
- [33] Drijckoning S, Janssens S D, Pobedinskas P, Koizumi S, van Bael M K and Haenen K 2016 The pressure sensitivity of wrinkled B-doped nanocrystalline diamond membranes *Sci. Rep.* **6** 35667
- [34] Bogdanowicz R, Ficek M, Sobaszek M, Nosek A, Gołuński Ł, Karczewski J, Jaramillo-Botero A, Goddard Iii W A, Bockrath M and Ossowski T 2019 Growth and isolation of large area boron-doped nanocrystalline diamond sheets: a route toward diamond-on-graphene heterojunction *Adv. Funct. Mater.* **29** 1805242
- [35] Bogdanowicz R, Ficek M, Malinowska N, Gupta S, Meek R, Niedziałkowski P, Rycewicz M, Sawczak M, Ryl J and Ossowski T 2020 Electrochemical performance of thin free-standing boron-doped diamond nanosheet electrodes *J. Electroanal. Chem.* **862** 114016
- [36] Rycewicz M, Ficek M, Gajewski K, Kunuku S, Karczewski J, Gotszalk T, Wlasny I, Wyszkołek A and Bogdanowicz R 2021 Low-strain sensor based on the flexible boron-doped diamond-polymer structures *Carbon* **173** 832–41
- [37] Rogers J A, Lagally M G and Nuzzo R G 2011 Synthesis, assembly and applications of semiconductor nanomembranes *Nature* **477** 45–53
- [38] Li L, Lin H, Qiao S, Zou Y, Danto S, Richardson K, Musgraves J D, Lu N and Hu J 2014 Integrated flexible chalcogenide glass photonic devices *Nat. Photon.* **8** 643–9
- [39] Rogers J A, Someya T and Huang Y 2010 Materials and mechanics for stretchable electronics *Science* **327** 1603
- [40] Chandran M and Hoffman A 2016 Diamond film deposition on WC-Co and steel substrates with a CrN interlayer for tribological applications *J. Phys. D: Appl. Phys.* **49** 213002
- [41] Ralchenko V G, Ashkinazi E E, Zavedeev E V, Khomich A A, Bolshakov A P, Ryzhkov S G, Sovyk D N, Shershulin V A, Yurov V Y and Rudnev V V 2016 High-rate ultrasonic polishing of polycrystalline diamond films *Diam. Relat. Mater.* **66** 171–6
- [42] Faili F, Palmer N, Oh S and Twitchen D 2017 Physical and thermal characterization of CVD diamond: a bottoms-up review 2017 16th IEEE Intersociety Conf. on Thermal and Thermomechanical Phenomena in Electronic Systems (ITherm) pp 1–7
- [43] Li H, Zhang T, Li L, Lü X, Li B, Jin Z and Zou G 2010 Investigation on crystalline structure, boron distribution, and residual stresses in freestanding boron-doped CVD diamond films *J. Cryst. Growth* **312** 1986–91
- [44] Pang H, Wang X, Zhang G, Chen H, Lv G and Yang S 2010 Characterization of diamond-like carbon films by SEM, XRD and Raman spectroscopy *Appl. Surf. Sci.* **256** 6403–7
- [45] Pandey M, D’Cunha R and Tyagi A K 2002 Defects in CVD diamond: Raman and XRD studies *J. Alloys. Compd.* **333** 260–5
- [46] Bernard M, Deneuille A and Muret P 2004 Non-destructive determination of the boron concentration of heavily doped metallic diamond thin films from Raman spectroscopy *Diam. Relat. Mater.* **13** 282–6
- [47] Knight D S and White W B 1989 Characterization of diamond films by Raman spectroscopy *J. Mater. Res.* **4** 385–93
- [48] Praver S and Nemanich R J 2004 Raman spectroscopy of diamond and doped diamond *Phil. Trans. R. Soc. A* **362** 2537–65
- [49] Solin S A and Ramdas A K 1970 Raman spectrum of diamond *Phys. Rev. B* **1** 1687–98
- [50] Eifert A, Langenwaller P, Higl J, Lindén M, Nebel C E, Mizaikoff B and Kranz C 2014 Focused ion beam (FIB)-induced changes in the electrochemical behavior of boron-doped diamond (BDD) electrodes *Electrochim. Acta* **130** 418–25

- [51] Živcová Z V, Frank O, Petrák V, Tarábková H, Vacík J, Nesládek M and Kavan L 2013 Electrochemistry and *in situ* Raman spectroelectrochemistry of low and high quality boron doped diamond layers in aqueous electrolyte solution *Electrochim. Acta* **87** 518–25
- [52] Mortet V, Gregora I, Taylor A, Lambert N, Ashcheulov P, Gedeonova Z and Hubik P 2020 New perspectives for heavily boron-doped diamond Raman spectrum analysis *Carbon* **168** 319–27
- [53] Szirmai P, Pichler T, Williams O A, Mandal S, Bäuerle C and Simon F 2012 A detailed analysis of the Raman spectra in superconducting boron doped nanocrystalline diamond *Phys. Status Solidi b* **249** 2656–9
- [54] Kononenko T V, Kononenko V V, Pimenov S M, Zavedeev E V, Konov V I, Romano V and Dumitru G 2005 Effects of pulse duration in laser processing of diamond-like carbon films *Diam. Relat. Mater.* **14** 1368–76
- [55] Cadot G B J, Billingham J and Axinte D A 2017 A study of surface swelling caused by graphitisation during pulsed laser ablation of carbon allotrope with high content of  $sp^3$  bounds *J. Phys. D: Appl. Phys.* **50** 245301
- [56] Medel A, Bustos E, Apátiga L M and Meas Y 2013 Surface activation of C- $sp^3$  in boron-doped diamond electrode *Electrocatalysis* **4** 189–95
- [57] Kankaanpää A, Meririnne E, Ariniemi K and Seppälä T 2001 Oxalic acid stabilizes dopamine, serotonin, and their metabolites in automated liquid chromatography with electrochemical detection *J. Chromatogr. B* **753** 413–9
- [58] Svorc L, Borovská K, Cinková K, Stanković D M and Planková A 2017 Advanced electrochemical platform for determination of cytostatic drug flutamide in various matrices using a boron-doped diamond electrode *Electrochim. Acta* **251** 621–30
- [59] Bennet K E *et al* 2016 A diamond-based electrode for detection of neurochemicals in the human brain *Front. Hum. Neurosci.* **10** 102
- [60] Li L *et al* 2018 Heterogeneous integration of microscale GaN light-emitting diodes and their electrical, optical, and thermal characteristics on flexible substrates *Adv. Mater. Technol.* **3** 1700239
- [61] Zhao Y *et al* 2019 Wirelessly operated, implantable optoelectronic probes for optogenetics in freely moving animals *IEEE Trans. Electron Devices* **66** 785–92
- [62] Chen P H, Lin C L, Liu Y K, Chung T Y and Liu C 2008 Diamond heat spreader layer for high-power thin-GaN light-emitting diodes *IEEE Photonics Technol. Lett.* **20** 845–7
- [63] Simon R B, Anaya J, Faili F, Balmer R, Williams G T, Twitchen D J and Kuball M 2016 Effect of grain size of polycrystalline diamond on its heat spreading properties *Appl. Phys. Express* **9** 061302
- [64] Yamamoto Y, Imai T, Tanabe K, Tsuno T, Kumazawa Y and Fujimori N 1997 The measurement of thermal properties of diamond *Diam. Relat. Mater.* **6** 1057–61
- [65] Graebner J E, Jin S, Kammlott G W, Herb J A and Gardinier C F 1992 Unusually high thermal conductivity in diamond films *Appl. Phys. Lett.* **60** 1576–8
- [66] Downey B P *et al* 2020 Micro-transfer printing of GaN HEMTs for heterogeneous integration and flexible RF circuit design *2020 Device Research Conf. (DRC)* pp 1–2
- [67] Almuslem A S, Shaikh S F and Hussain M M 2019 Flexible and stretchable electronics for harsh-environmental applications *Adv. Mater. Technol.* **4** 1900145
- [68] Cumont A, Pitt A R, Lambert P A, Oggioni M R and Ye H 2021 Properties, mechanism and applications of diamond as an antibacterial material *Funct. Diam.* **1** 1–28
- [69] Cumont A, Zhang R, Corscadden L, Pan J, Zheng Y and Ye H 2020 Characterisation and antibacterial investigation of a novel coating consisting of mushroom microstructures and HFCVD graphite *Mater. Des.* **189** 108498
- [70] Sharma D, Jia W, Long F, Pati S, Chen Q, Qyang Y, Lee B, Choi C K and Zhao F 2019 Polydopamine and collagen coated micro-grated polydimethylsiloxane for human mesenchymal stem cell culture *Bioact. Mater.* **4** 142–50